Millimeter wave spectroscopy of propynal isotopologues and structure determination

E.G. Robertson, M. Ruzi, D. Mcnaughton, L. Margulès, R.A. Motiyenko, J. C. Guillemin

Millimeter wave Spectroscopy of Propynal Isotopologues and Structure Determination

Evan G. Robertson[1*], Mahmut Ruzi[1,2], Don McNaughton[3], Laurent Margulès[4], Roman A. Motiyenko[4], Jean-Claude Guillemin[5].

1. Department of Biochemistry & Chemistry, La Trobe Institute of Molecular Sciences, La Trobe University, Victoria 3086, Australia
2. ERNAM - Nanotechnology Research and Application Centre, Erciyes University, Kayseri 38039, Turkey
3. School of Chemistry, Monash University, Wellington Road, Clayton, Victoria, 3800, Australia.
4. PhLAM - Physique des Lasers Atomes et Molécules, University of Lille, UMR 8523 - CNRS, F-59000 Lille, France.
5. Univ Rennes, Ecole Nationale Supérieure de Chimie de Rennes, CNRS, IRCR-UMR 6226, F-35000 Rennes, France

* Corresponding author: e.robertson@latrobe.edu.au

Abstract

Rotational transitions of propynal (HCCCHO) have been measured in the 150-900 GHz region by millimeter wave spectroscopy and in the far infrared region by high resolution FTIR spectroscopy using a synchrotron source. For the parent isotopologue, assignment of MMW transitions up to very high quantum numbers (J = 100, K_a = 25) reveals evidence of extensive perturbations in the ground vibrational state due to Fermi-asymmetry resonance with an excited vibrational state. A fit to nearly 3000 ground state transitions yields effective constants that are suitable for describing relatively unperturbed rotational levels up to K_a = 13. Over 1000 transitions were assigned and fitted for each singly substituted ^{13}C species and nearly 400 transitions for the ^{18}O variant. Re-analysis of literature data on deuterated species, aided by centrifugal distortion constants from hybrid density functional theory calculations at the B2PLYP/aug-cc-pVTZ level, provides a further set of rotational constants. This allows determination of a $R_m^{(2)}$ structure for propynal with the following geometry: r(C≡C) = 1.2066(15), r(C-C) = 1.4486(14), r(CO) = 1.2087(10), r(C-H ald) = 1.1069(8), r(C-H acet) = 1.0578(13), θ(CCC) = 176.71(22), θ(OCC) = 123.23(7), θ(HCC ald) = 114.43(31), θ(HCC acet) = 178.45(16). A new R_s structure was also derived.

Keywords: Propynal, millimeter wave spectroscopy, far-IR spectroscopy, interstellar medium, isotopic substitution, molecular structure, density function theory, ab initio calculations.

Introduction

Propynal (HCCCHO) was first detected in the interstellar medium (TMC-1) in 1987, by Irvine et al [1]. This was followed by several other interstellar microwave observations [2–6] and in the millimeter-wave region by Loison et al [7]. It is noteworthy that of the three stable H_2C_3O isomers, thermodynamically favoured propadienone has so far eluded astronomical observation. Detection of both of the other two isomers, propynal and cyclopropenone, in interstellar molecular clouds suggests that kinetic rather than thermodynamic factors control the abundances of these H_2C_3O species [6,7] and kinetic modelling suggests propynal is formed via the reaction of O + C_3H_3 reaction [7]. However, faster decomposition may also explain the lack of the other H_2C_3O isomer, propadienone [8].

The astronomical observations rely on accurately known line positions obtained directly from laboratory-based measurements or predicted from very well determined molecular constants. Beginning in the 1950's, a series of studies have led to steadily improving molecular constants for propynal's parent isotopologue, with the assignment of microwave [9–11] and millimeter wave [12,13] transitions up to 200 GHz. Barros et al used coherent synchrotron radiation to measure FTIR spectra in the 250-700 GHz range with a resolution of 30 MHz, and refined the ground state constants by combining their assignments with previous MW data [14]. The permanent dipole moment components along the a- and b-axis of propynal (see figure 1), relevant to intensity or concentration calculations, were determined via Stark effect measurements carried out by Brown and Godfrey [15].
A few transitions from excited vibrational states were examined by MW-IR double resonance [16,17], before McKellar et al [18] undertook a detailed high resolution FTIR study of the ν_7, ν_8, and ν_{11} bands in the 570 – 740 cm^{-1} region.

Apart from the parent isotopologue, Costain & Morton's microwave work encompassed transitions from HCCCHO species with one ^{13}C or ^{18}O atom in natural abundance and from species in deuterated samples, which facilitated determination of a substitution structure [10]. For DCCCHO, a more extensive set of transitions from the millimeter-wave region has been reported [19]. In an astrochemical context, isotopic ratios are of considerable interest due to significant spatial variation. For example, the $^{12}C/^{13}C$ ratio, which is *ca*. 90 on earth, was found from millimeter wave data on CO to range from 24 in the centre of our galaxy to *ca*. 70 at 12 kiloparsec [20].

The findings presented here have their origin with high resolution FTIR spectroscopy measurements at the Australian synchrotron over a decade ago. From ongoing analysis of far infrared bands, it became evident that the low-lying vibrational states and also the ground state of propynal were affected by a number of resonance perturbations which greatly complicate a comprehensive rovibrational analysis. To improve the description of these vibrational states of propynal, in 2014 further experiments were performed by millimeter wave spectroscopy in the 150 – 900 GHz region. The sensitivity of these measurements permitted analysis of several isotopologues of propynal in natural abundance. In parallel, recent work by Jabri et al [21] have described millimeter wave measurements to 480 GHz and analysed a number of isotopologues and vibrational states. It provides a useful point of comparison to the present work. Here, we focus on the ground vibrational

state but extend on what is reported already by assigning and fitting more transitions with a greater range of quantum numbers. The analysis is supported by comparison with high level anharmonic theoretical calculations. Literature data from further isotopologues is subject to re-examination, and the improved set of rotational constants used in structural analyses. A variety of methods are explored, culminating in a $R_m^{(2)}$ structure.

Experimental

For infrared spectroscopy, propynal was synthesised following a convenient method outlined by McNab et al [22]. The pyrolysis products of diprop-2-ynyl ether are trapped at liquid nitrogen temperature, and then warmed to room temperature so that the more volatile allene (propadiene) may be removed by pumping, leaving almost pure propynal liquid. For millimeter wave spectroscopy experiments performed in Lille, a pure sample was prepared in Rennes using the synthesis of Sauer [23], transferred to Lille in dry ice then stored under nitrogen at a temperature below -20°C.

Millimeter wave spectroscopy

Absorption spectra of propynal were measured on a fast-scan terahertz spectrometer in Lille. The spectrometer itself and the fast scan system have been described in detail previously [24,25]. The absorption cell was a stainless-steel tube (6 cm in diameter, 220 cm in length). The sample was at room temperature, with a pressure during measurements of *ca*. 10 Pa, and the line width was limited by Doppler broadening. The frequency range was covered with various active and passive frequency multipliers from VDI Inc. and an Agilent synthesizer (12.5-18.25 GHz) was used as the source of radiation. Absorption signals were detected by an InSb liquid He-cooled bolometer (QMC Instruments Ltd.). Spectra were measured in five separate regions between 150 – 910 GHz covering a total of 510 GHz. The data point intervals correspond to approximately 5% of the linewidth in each region, see supplementary data table S1. Peaks appear as the 2nd derivative of a Voigt profile.

Millimeter wave spectra were subjected to 9-point Savitzky-Golay smoothing to reduce the point to point noise. Peak positions, amplitudes and widths were obtained using the second derivative peak search method in OPUS, with the 17-point Savitzky-Golay algorithm used to obtain the derivatives. High signal to noise ratio in the spectra (*ca* 1000:1) allowed the detection of nearly 75000 peaks. The accuracy with which the peak positions may be determined depends primarily on their linewidths, which increase with frequency since Doppler broadening represents the major contribution. High quality peaks (just over a third of the total) were assigned a default uncertainty corresponding to approximately 5% of the median linewidth of peaks in that region, see table S1. The uncertainties of other peaks were scaled by cumulative multipliers (x2 or x4) pertaining to various criteria: very high intensity giving rise to saturation, low intensity, anomalously high linewidths, overlap with nearby lines close enough to affect the determination of peak centre, or assignment as an unresolved shoulder by the peak pick algorithm. Transitions taken from the literature were assigned an uncertainty of 0.10 MHz.

Far IR Spectroscopy

A limited set of 25 far IR rotational transitions was ultimately used in this work, so a brief outline only is provided here. Far IR measurements were performed at the Australian synchrotron, using synchrotron edge radiation as the source and a Bruker IFS 125HR spectrometer operating with a silicon bolometer, and 6 micron mylar beamsplitter. Spectra were measured at maximum instrument resolution of 0.00096 cm^{-1} and transformed using the inbuilt 4P apodisation function. Separate sets of 74 and 91 scans were obtained with propynal at pressures 7.3 and 139 Pa respectively in a 0.60 m White cell set to 8 passes for 4.8 m pathlength. The IR spectra were calibrated by comparison with water line positions from the HITRAN database [26].

Results

Assignment and fitting of the parent isotopologue

Pickett's SPFIT/SPCAT programs [27] were used for fitting and prediction, using Watson's s-reduced Hamiltonian [28]. Rotational lines of the unsubstituted parent species reported in the literature [10,12,13], when refitted, provided an initial set of molecular constants used to predict further transitions. Propynal has dipole moment components of μ_a = 2.36±0.02 D, μ_b = 1.47±0.02 D [15], giving rise to both a-type and b-type rotational transitions. The predicted transitions were ordered in series with K_a quantum number in common, and new assignments made by considering both the frequency and relative intensity of the observed peaks.

Assignment was conducted in an iterative manner, with rotational and centrifugal distortion constants refined as more observed transitions were accrued. All together, nearly 4000 MMW transitions were assigned (including 1000 degenerate pairs differing in K_c only). These extended up to J = 100 and K_a = 25, far beyond the range of previously assigned microwave or millimeter wave lines. The $\Delta K_a = \pm 1$ selection rule of b-type transitions shifts them to higher frequency as K_a increases, so the 910 GHz maximum frequency of the present experiments limit their assignment to $K_a' = 13$ (found in ${}^{r}P_{12}$ transitions, using the notation ${}^{\Delta Ka}\Delta J_{Ka''}$).

Plots of (observed – calculated) residuals vs quantum number reveal perturbations in the rotational levels of the ground vibration state, see figure 2. These have not been alluded to in previous propynal studies, presumably due to the more limited quantum number ranges. Perturbations affecting the ground vibrational state are not commonly detected, but they have been noted in near-prolate molecules with very large A rotational constants and low frequency bending modes like ketene (H_2CCO) and diazomethane (H_2CNN) [29], thioketene (H_2CCS) [30] and ketenimine [31], and $HOCO^+$ [32].

Preliminary analysis of the millimeter wave and far IR spectra of propynal in the realm of ν_9 at 205.2 cm^{-1} and ν_{12} at 260.5 cm^{-1} allows the perturbing levels to be positively identified. Energy levels come into close proximity leading to detectable perturbations that increase with J in the following K_a quantum number regions:

- $K_a = 10$ (ground state) ↔ $K_a = 2$ (ν_9), a weak perturbation detectable only at high J;
- $K_a = 14$ (ground state) ↔ $K_a = 10$ (ν_9) ↔ K_a 8 (ν_{12}), causing significant perturbation for $J > 40$;
- $K_a = 25$ (ground state) ↔ $K_a = 23$ (ν_9), resulting in pervasive perturbations that affect K_a 20-30.

These are all consistent with Fermi-like asymmetry resonances (with ΔK_a and ΔK_c even) between the ground state and ν_9, both of A' symmetry. The A' ν_9 and A'' ν_{12} states are strongly a-axis Coriolis coupled to each other and in turn to higher states, so that a comprehensive fit to the ground vibrational state requires simultaneous treatment of ν_9, ν_{12}, $2\nu_9$, $\nu_9+\nu_{12}$, and $2\nu_{12}$. Such an analysis is in progress, but for the present, an effective fit to the ground state only is considered.

It is therefore necessary to restrict transitions to those with $K_a \leq 13$ whose energy levels are not seriously perturbed, see figure 2 and table 1. The final set of transitions fitted includes 2985 MMW lines from the present work (512 of which are degenerate pairs differing in K_c only), and 101 microwave transitions from previous studies. A limited set of 25 b-type rotational lines from the far IR spectrum with K_a up to 31 was also included to assist the determination of higher order K_a dependent centrifugal distortion parameters. By selecting transitions involving only J - $K_a = 0$ levels (e.g. $30_{30,0} \leftarrow 29_{29,1}$) the perturbing effects of second order Coriolis and asymmetry resonances are minimised.

Due to the large number of transitions and their wide quantum number range it was possible to determine all the quartic (D, d), sextic (H, h) and octic (L, l) centrifugal distortion constants, some 10^{th} order P terms and the 12^{th} order T_K. These constants, listed in table 2, satisfactorily reproduce the included transitions to a rms deviation of 40 kHz, while the overall rms error for the weighted fit was 0.52. The agreement with the constants from Jabri et al [21], derived from a different though overlapping set of lines, is generally excellent up to the 6^{th} order terms and even the 8^{th} order L constants are within about 20%. Due to the greater range of quantum numbers incorporated in the present fit, the parameters have smaller uncertainties and more of the higher order constants can be determined.

While the present effective fit does not account for the ground state perturbations at higher K_a values, it does accurately reproduce the energy levels within the K_a 0-13 range that are likely to be accessible in rovibrational analyses of FTIR bands at room temperature or in astrochemical surveys. The computed spectrum is available in standard .cat format [27] from the Lille Spectroscopic Database (https://lsd.univ-lille.fr), which allows predictions to be generated using customisable intensity units, temperature, and frequency range.

Comparison with theoretical calculations

Harmonic and anharmonic vibrational calculations were carried out using the Gaussian suite [33] to support the spectroscopic analysis of isotopologue spectra and geometry determination. The levels of theory employed included MP2, B3LYP, M062X, B2PLYPD3 and DSDPBEP86, with basis sets up to aug-cc-pVTZ for each. At CCSD(T)/cc-pVTZ level, only geometry optimisation was possible due to computing resource limitations. A recent study presented similar calculations using MP2, B3LYP, CAM-B3LYP and ωB97XD levels of theory [34]. In the final stages of writing up the present work, a new paper from Tschöpe and Rauhut was released reporting very high level

CCSD(T)/cc-pVTZ-F12 anharmonic calculations applied to rovibrational spectroscopic properties of propynal [35].

Leaving aside the very latest CCSD(T)/cc-pVTZ-F12 calculations, we found that B2PLYPD3 and DSDPBEP86, both double hybrid density functional theory methods incorporating HF exchange and perturbative second-order electron correlation, provide the best overall performance in matching experimental spectroscopic data of propynal. For example, the RMS deviation between experimental band positions and corresponding anharmonic predictions is just 12 and 10 cm^{-1} at these levels (see supplementary data table S3). The zero-point corrected rotational constants at B2PLYPD3 and DSDPBEP86 levels, reflecting the ground state geometry, are within 0.5% of the experimental values and so are the Δ_0 inertial defects (see table 3). For the other levels of theory, the B_0 and C_0 constants are within 1% of experiment but the A_0 constants are either underpredicted (MP2) and overpredicted (DFT) by more than this margin. It is evident from table 3 that B2PLYPD3 and DSDPBEP86 centrifugal distortion parameters are also well predicted, which is useful in the context of fits to isotopologue with limited transition sets as detailed later.

^{13}C and ^{18}O isotopologues

The high signal-to-noise ratio of the millimeter wave spectra enabled observation of singly substituted isotopologues in natural abundance, i.e. 1.1% for ^{13}C and 0.21% for ^{18}O, as seen for example in figure 3. Initial rotational assignments were guided by Costain & Morton's rotational constants [10] and then progressively refitting as more lines were assigned. For each of the three ^{13}C species, a-type and b-type transitions were observed, totalling over 1000 and ranging up to J_{max} ≈ 67 and $K_{a\,max}$ ≈ 16. These showed evidence for similar perturbations to those affecting the parent species, but the more limited set of transitions meant that only a few had to be excluded from the fits: those with $K_a > 13$ where $J > 40$. For the less abundant ^{18}O species, only a-type lines could be observed up to J_{max} ≈ 57 and $K_{a\,max}$ ≈ 15.

The fitted parameters are summarised in table 2, while the SPFIT lists of transitions and output files are available as supplementary data files, summarised in table S2. The approach taken was to float the centrifugal distortion parameters that could be well determined and fix the remaining higher order ones to the values from the ^{12}C species. The RMS deviations of the fits were around 40 kHz, well within the uncertainty of most of the peak frequencies.

Costain & Morton did not fit the A rotational constants to these species due to the absence of b-type lines in their limited data set, but their B and C constants are close to the newly refined set. In the more recent work of Jabri et al [21], the ^{18}O isotopologue was not studied but *ca*. 200 a-type lines were assigned for each of the ^{13}C species, up to $J_{max} = 36$ and $K_{a\,max} = 13$ or 16. Their fits include constants up to sextic centrifugal distortion. The agreement between those parameters and the corresponding ones in the present fit is generally excellent except for K_a dependent parameters (A, D_K and H_K), largely as a consequence of them not detecting b-type lines to constrain the energy gaps between K_a levels.

Deuterated isotopologues

With an objective of conducting structural analysis of propynal, it was desirable to secure rotational constants for deuterated species. These were not detectable in the natural abundance spectrum (D 0.016%), but further fits were carried out using the data of Costain & Morton [10].

In the case of DCCCHO only, Takami also measured a more extensive set of rotational transitions up to J_{max} = 34 and $K_{a\,max}$ = 18, although lines with K_a 16-18 were excluded from his analysis due to large residuals [19]. Incorporating Costain & Morton's 11 lines and 142 transitions with K_a <16 from Takami, we have refitted the data to Watson's s-reduced Hamiltonian, see table 4. As with the ^{13}C and ^{18}O species, higher order centrifugal distortion constants that could not be well determined were fixed to those of the ^{12}C species. The RMS deviation of the transitions was 50 kHz, a modest improvement on the 61 kHz deviation obtained if the constrained parameters are omitted entirely.

For each of the isotopologues, HCCCDO, DCCCDO, D^{13}CCCHO, DC^{13}CCHO and DCC^{13}CHO, Costain & Morton report 6-8 transitions with low values of J and K_a [10]. Their original treatment made an approximate determination of two quartic centrifugal distortion constants only, D_J = 2.0×10^{-3} MHz and D_{JK} = -0.141 MHz. Even in this low J range, quartic centrifugal distortion makes a significant contribution of several MHz to transition frequencies. It is therefore important to incorporate it satisfactorily, despite having insufficient data to reliably fit the associated parameters. A reasonable approach would be to use the values from the ^{12}C species, although we note that the quartic parameters of ^{13}C and ^{18}O species in table 2 differ from the ^{12}C species by up to 10%. Alternatively, the parameters could be taken directly from theoretical calculations for that isotopologue. A third possibility, the approach used here, is to extrapolate from the observed experimental values of the parent isotopologue by scaling with the computed ratio found for those species. E.g.

$$D_J(\mathrm{HCCCDO}) \approx D_J(\mathrm{HCCCHO\ exp}) \times \frac{D_J(\mathrm{HCCCDO\ comp})}{D_J(\mathrm{HCCCHO\ comp})} \qquad (1)$$

To gauge the reliability of this approach, ratios computed at the anharmonic B2PLYPD3/aug-cc-pVTZ level were used to extrapolate values for the twenty quartic constants of the four undeuterated ^{13}C and ^{18}O species. The resulting predictions are within 1% of the fitted values in table 2, except for the d_2 constant H^{13}CCCHO which is underestimated by 2% (refer to supplementary data table S4).

Table 4 presents the extrapolated centrifugal distortion constants for five further deuterated species, and the rotational constants determined from refitting Costain & Morton's transitions [10]. The aldehyde hydrogen is the atom furthest from the principal a-axis of propynal (see figure 1), so deuteration at that position has the most significant effect on the fitted A rotational constants of HCCCDO and DCCCDO (reduced by *ca*. 24%). Isotopic effects on the moments of inertia reflected in the rotational constants are expected to be further amplified in the corresponding centrifugal distortion constants, as illustrated in the simple case of a diatomic molecule, where $D_J = 4\,B_e^3/\omega_e^2$. Accordingly, the extrapolated D_{JK} and D_K constants of HCCCDO and DCCCDO are also greatly reduced in magnitude, by *ca*. 60%. The RMS deviation of transition frequencies is 18 kHz for the HCCCDO fit and 31 kHz for DCCCDO, validating the approach taken as the RMS deviations increase to over 200 kHz if quartic constants from the unsubstituted isotopologue are used instead.

The A constants in these two species are 4 MHz higher than Costain & Morton's values, while B and C are higher by *ca*. 0.10 MHz and 0.05 MHz respectively, showing that the refits are justified.

For the three remaining isotopologues, D^{13}CCCHO, DC^{13}CCHO and DCC^{13}CHO, the A constants could not be determined as no b-type transitions were available. These were instead constrained to values extrapolated from the isotopologue DCCCHO, scaled by the computed ratio at anharmonic B2PLYPD3/aug-cc-pVTZ level found for those species. For example,

$$A_0(\mathrm{H^{13}CCCDO}) \approx A_0(\mathrm{HCCCDO\ exp}) \times \frac{A_0(\mathrm{H^{13}CCCDO\ comp})}{A_0(\mathrm{HCCCDO\ comp})} \qquad (2)$$

Similar extrapolation between the undeuterated ^{13}C-substituted species in table 2 and unsubstituted HCCCHO produces A_0 constants within 7 MHz (0.010%) of experimental values. This indicates that the extrapolated A_0 constants of D^{13}CCCHO, DC^{13}CCHO and DCC^{13}CHO are probably within 15 MHz of their true values. The transition sets for these three species, unlike HCCCDO and DCCCDO, extend to $K_a = 2$. This allows B and C to be determined along with one quartic term, D_{JK}. The fitted D_{JK} constants are physically realistic, differing from the extrapolated values by a few percent only. The RMS deviations of transition frequencies are *ca*. 60 kHz, considerably less than the 150 kHz reported by Costain & Morton for the associated J = 3←2 transitions. The refitted B and C constants differ from the earlier ones by 0.02 – 0.06 MHz.

Finally, Costain & Morton also measured two or three transitions each for some more aldehyde deuterated species: H^{13}CCCDO, HC^{13}CCDO, HCC^{13}CDO and HCCCD^{18}O. New fits have been conducted, again using extrapolated B2PLYPD3/aug-cc-pVTZ centrifugal distortion constants. The refitted B and C constants exceed the earlier ones by 0.07-0.09 MHz, refer to supplementary data table S5.

Structure Determination

Costain & Morton derived an R_s substitution structure based on the average from separate analyses of three data sets: the undeuterated, acetylenic-deuterated, and aldehyde-deuterated species [10]. For comparison, using the KRA and EVAL software [38] we derived an R_s structure from the new A and B rotational constants of the parent species together with the six singly substituted isotopologues. Unlike the previous analysis, the $\theta_{\mathrm{HCC\ acet}}$ angle was not constrained to 180.0° and a slightly non-linear value of 178.88° was obtained (see table 5). Probably associated with that change, the adjacent θ_{CCC} angle was reduced from 178.40° to 177.39°. The $r_{C1\equiv C2}$ and $r_{C3=O}$ bond distances also decreased by 0.002-0.003 Å. The new R_s structure is a better overall match to the theoretical structures of table 5.

R_s derived structures are considered intermediate between the vibrationless R_e equilibrium structure and R_0 geometries in the zero-point level, which vary slightly with isotopic composition. Ultimately, it is useful to derive equilibrium structures instead, which in principle are isotope independent and directly comparable to optimised potential energy minima structures from *ab initio* calculations such as those presented in table 5.

In the absence of a complete set of experimental rovibrational α values for all isotopologues to enable a definitive R_e structure determination, different approaches are possible. Rovibrational α values from quantum chemical or DFT calculations may be used to derive estimated R_e constants and derive a "semi-empirical" R_e structure. Alternatively, Watson et al proposed incorporating mass-dependant corrections to the zero-point moments of inertia [36]. The $R_m^{(2)}$ model generally allows much better fits and the resultant geometric parameters correspond fairly closely to those of the equilibrium structure. The formulation of this adopted by Kisiel [37] and implemented in the least squares fitting software STRFIT [38] is:

$$I_0^\alpha = I_m^\alpha + c_\alpha (I_m^\alpha)^{1/2} + d_\alpha (m_1 m_1 ... m_N / M)^{1/(2N-2)} \quad \text{equation 1}$$

I_0^α are the measured moments of inertia about the principal axes, α = a, b, c. I_m^α are the rigid moments of inertia calculated directly from the internal coordinates to be fitted. m_i are the masses of the constituent atoms, M is the total mass of the molecule, and N is the number of atoms in the molecule. The coefficients c_α and d_α are the $R_m^{(1)}$ and $R_m^{(2)}$ parameters.

The rotational analyses reported in tables 2 and 4 have yielded a large set of 30 well determined rotational constants (11 *B*, 11 *C* and 8 *A* constants) for different isotopologues. For details, refer to supplementary table S6. The four aldehyde deuterated species of supplementary data table S5 also provide *B* and *C* values, but their uncertainties are larger due to the minimal number of transitions available. Consequently, they were not included in the structural fits but were used as a secondary data set to test the robustness of those fits. In the present work, a number of trials were performed using the STRFIT software to assess how well the structural parameter sets could fit the observed moments of inertia, equally weighted. In these fits outlined below, the constraint of planarity was imposed. Although in a few cases allowing non planarity produced slightly improved fit deviations, the theoretical geometry calculations provided strong support for a planar potential energy minimum. The DFT double hybrid B2PLYPD3/aug-cc-pVTZ and DSDPBEP86/aug-cc-pVTZ methods from this study are reasonably high levels of theory and even more so the *ab initio* CCSD(T)/cc-pVTZ-F12 method employed by Tschöpe & Rauhut [35]. Close agreement between the three sets of computed structural parameters (see table 5) lends credibility to their predictions, so that to an extent they can be used to assess the various fitted structures.

(a) As an initial reference, a basic "R_0 structure" fit gives a very large residual standard deviation of 0.0680 amu.Å^2 for the moments of inertia which is characteristic of a poor fit as expected when taking no account of zero-point vibrational motion.

(b) Considering the semi-empirical approach, a level of theory must be selected likely to provide reliable rovibrational contributions, ½ Σα . In the harmonic approximation, the summed α contributions from B2PLYPD3, DSDPBEP86, B3LYP, M062X and MP2 levels of theory (all with aug-cc-pVTZ basis) were quite consistent, e.g. ½ $\Sigma\alpha_a$ = -737 ±10, ½ $\Sigma\alpha_b$ = -4.2 ±0.1, ½ $\Sigma\alpha_c$ = -0.1 ±0.2 MHz for the parent isotopologue HCCCHO. Anharmonic contributions are likely to be important, but the corresponding Σα values were found to be highly variable, e.g. ½ $\Sigma\alpha_a$ ranged from +83 (MP2) to -1404 (M06-2X) MHz. Trial fits using harmonic or anharmonic ½ Σα values

from B2PLYPD3 (see fitted structure reported as "Semi-emp" in table 5) and DSDPBEP86 calculations yielded residual standard deviations of *ca*. 0.0028 amu.Å^2. This is an order of magnitude better than the "R_0" fit but still only moderately satisfactory in that the deviations remain much larger than experimental uncertainties. The structural parameters are in reasonable agreement with theoretical R_e values in table 5, except that near-linear acetylenic HCC angles of 180.2° are somewhat larger than the theoretical results (of 178.8°) suggest.

(c) An $R_m^{(1)}$ fit that accounts for the three c_α coefficients gives a residual standard deviation of 0.0032 amu.Å^2, with geometric parameters listed in supplementary data table S7. The fitted c_a value is nearly zero, but c_b and c_c, which have positive sign and are of modest magnitude, help to improve the fit considerably. The $R_m^{(1)}$ fit of acrylonitrile (H_2C=CHCN), a molecule of comparable size and bonding arrangement to propynal, gives very similar standard deviation (0.0031 amu.Å^2) and c_α coefficients (-0.0097, 0.0271, 0.0381 amu$^{1/2}$.Å^2) [39]. The $R_m^{(1)}$ geometry of propynal is quite consistent with the R_s structures and to a lesser extent with the theoretical R_e predictions. However, some significantly large and systematic (obs – calc) residuals remain.

(d) An $R_m^{(2)}$ fit incorporating c_α and the mass-dependant d_α coefficients produces a slightly smaller residual standard deviation of 0.0024 amu.Å^2 (fitted structure reported as "$R_m^{(2)}$ poor" in supplementary data table S7), but there are some issues. Firstly, the c_α constants are an order of magnitude larger than in the $R_m^{(1)}$ fit and the highly correlated d_b and d_c constants have questionably large magnitudes (*ca*. -1.2 Å^2). Secondly, the fitted parameters do not closely predict the I_b and I_c values for the secondary test set of four aldehyde D-substituted ^{13}C/^{18}O species, giving RMS residuals of 0.0044 amu.Å^2. Thirdly, the fitted internal coordinates differ substantially from the theoretical predictions of table 5 (some bond distances by more than 2 pm and the aldehyde HC3C2 angle by over 3°). In that respect, the $R_m^{(2)}$ geometry appears worse than $R_m^{(1)}$ (with bond distances within 1.1 pm and the aldehyde HC3C2 angle out by 1.5°).

(e) Laurie-type correction parameters are often used to account for the reduction difference in bond distance when hydrogen is substituted for deuterium [36,40]. Typically, r_0(CH) – r_0(CD) ≈ 0.003 Å. Applied here to the acetylenic CH bond distance, the $R_m^{(2L)}$ fit deviation is much reduced (to 0.00088 amu.Å^2) but the value of fitted Laurie parameter (-0.17 Å) implies r_{CD} is around 0.05 Å longer. This is physically unrealistic, having the opposite sign and being an order of magnitude larger than expected, suggesting that here it is serving only as an effective correction parameter that does not realistically describe the isotopically induced geometry changes occurring in the zero-point levels.

Examination of the largest (obs – calc) residuals from the $R_m^{(1)}$ fit gives some insight into the nature of the problem with the structure fits. The I_b residuals for the aldehyde C3-substituted species HCC^{13}CHO and DCC^{13}CHO are large and negative (-0.006 amu.Å^2), while those for the C2-substituted species HC^{13}CCHO and DC^{13}CCHO have the opposite sign (+0.005 amu.Å^2).
The anharmonic frequency calculations are broadly consistent with this trend: at both B2PLYPD3 and DSDPBEP86 levels the ½ $\Sigma\alpha_b$ value for HC^{13}CCHO exceeds that of HCC^{13}CHO by 0.37 MHz, corresponding to ΔI_b = 0.008 amu.Å^2. The difference for the corresponding DCCCHO species is

0.35 MHz (ΔI_b = 0.009 amu.Å^2). Similar experimental and calculated DFT trends are found for HCCCDO species in the secondary (unfitted) data set. The experimental *B* (and *C*) rotational constants of ^{13}C3 vs ^{13}C2 substituted species differ by only a few MHz (see tables 2, 4), because those two atoms are located at almost the same distance from the b-principal axis (see figure 1). As a consequence, ΔI_b from their c_b terms in equation 1 will be virtually identical. Neither can the d_α coefficients produce the required difference because changing the position of ^{13}C substitution does not alter those terms in the equation 1.

(f) Fitting 30 experimental moments of inertia to determine 12 internal coordinates (and up to 6 $R_m^{(2)}$ parameters) provides a level of redundancy, such that some of that data could be omitted. It is instructive to note what occurs if the aldehyde ^{13}C3-substituted species are excluded, so that only 9 isotopic species (with 25 moments of inertia) are fitted. The deviation of the $R_m^{(2)}$ fit is drastically improved to 0.00059 amu.Å^2. The six c_α and d_α constants are reduced in magnitude by a factor of at least 5. Predictions for H^{13}CCCDO, HC^{13}CCDO and HCC^{13}CDO (but not HCCCD^{18}O) in the secondary set give RMS residuals of 0.0019 amu.Å^2. A fit of similar quality may be obtained by excluding the ^{13}C2 variants HC^{13}CCHO and DC^{13}CCHO instead (0.00056 amu.Å^2). The outcome is less satisfactory if H^{13}CCCHO and D^{13}CCCHO are omitted instead. Although the fit deviation of 0.00044 amu.Å^2 is low, the I_b and I_c residuals for the omitted ^{13}C1 species (at over 0.03 amu.Å^2) are three times greater than was found for omitted ^{13}C species in the other two fits and an anomalously short r_{C1C2} distance of 1.197 Å is obtained. The geometric parameters from the first two fits, omitting ^{13}C2 and ^{13}C3 species in turn, are fairly consistent except for the r_{C2C3} distance, 1.439 Å and 1.456 Å respectively. Averaging the structural parameters of these two fits, the geometry reported as "$R_m^{(2)}$ fit 9 av" in supplementary data table S7 is obtained. A drawback is that the indicative structure does not directly allow prediction of the rotational constants for each isotopologue.

(g) As an alternative to excluding ^{13}C2 or ^{13}C3 substituted data, a geometric correction may be applied to the internal coordinates of those particular species to allow their inclusion in the fit and provide some insight into the magnitude of the zero-point geometry changes involved. In a series of trial fits applying one consistent correction to both ^{13}C3-substituted species, much improved fit deviations of *ca*. 0.0006 amu.Å^2 were obtained by a small change in r_{C2C3} distance (by -0.00017 Å), or in the θ_{OC3C2} angle (by -0.016 °), or the θ_{C3C2C1} angle (by +0.040 °). Correcting the r_{C2C3} distance (by +0.00017 Å) of the ^{13}C2 species instead yielded a similar improvement. Finally, as a compromise to minimise distorting effects, a half size r_{C2C3} distance correction was applied to both ^{13}C2 (+0.000085 Å) and ^{13}C3 species (-0.000085 Å). The r_{C2C3} distance corrections applied are much smaller than the uncertainty then determined for the r_{C2C3} distance, 1.4486±0.0014 Å.

This fit, labelled "$R_m^{(2)}$ (ΔC_2C_3)" in the table 5 summary (and detailed further in supplementary table S6), may be considered satisfactory and the resulting structure reliable by a number of criteria. It has a low deviation of 0.00062 amu.Å^2. The c_α and d_α constants are an order of magnitude smaller than those from the uncorrected $R_m^{(2)}$ fit. I_b and I_c predictions for the unfitted secondary set species H^{13}CCCDO, HC^{13}CCDO, and HCC^{13}CDO (with geometry correction applied to the latter two) give RMS residuals of 0.00062 amu.Å^2 well within their experimental uncertainties, although

HCCCD^{18}O is not so well predicted. The internal coordinates are very similar to those from the "$R_m^{(2)}$ fit 9 av" geometry and largely consistent with those from the B2PLYPD3, DSDPBEP86 and CCSD(T) calculations presented in table 5. Compared to the CCSD(T) geometry, the CC and CO bond distances are within 0.002 Å, CH distances within 0.008 Å, while the largest bond angle discrepancy is 0.9 degrees for θ_{CCC}.

Discussion and Conclusions

Measurements using a highly sensitive millimeter wave spectrometer, together with FTIR spectroscopy with a synchrotron source, have facilitated the assignment of thousands of rotational transitions in propynal. This has extended the range of accessible quantum numbers in both the parent species and other isotopologues. Over 1000 millimeter wave transitions were assigned and fitted for each of the three singly substituted ^{13}C species, and 371 for the ^{18}O variant, despite it being present at just 0.2% in natural abundance.

The assignment of over 4000 lines of the parent species up to J = 100 and K_a = 25 has revealed pervasive perturbations affecting the ground vibrational state levels beyond K_a = 13. The strongest effects are found in K_a = 25 levels with J over 50, where far IR rotational transitions reveal shifts of more than 1 cm^{-1} (30 GHz). Such interactions are rarely detected, because of the requirement for interacting rotational levels of a ground and excited vibrational state to come into close enough proximity. The few known examples involve molecules that are near linear, with large A rotational constants. In the case of propynal, a significant a-axis Coriolis interaction between CCC bending modes ν_9 and ν_{12} serves to reduce the effective A_9 constant (to 63434 MHz [21]), thereby helping to close the energy gap between ground state and ν_9 levels and amplify the effect of resonance interactions between them. This Fermi-like asymmetry interaction will affect not only the ground vibrational state. Every vibrational state of the molecule can interact similarly with the state possessing one more quantum of ν_9, $N_v \leftrightarrow N_v 9_1$.

In the ground state, perturbations are minimal for K_a 0-12 and low J levels of K_a = 13, which allows for an effective one state fit where higher order centrifugal distortion parameters can account for omission of the relevant interaction terms within that quantum number range. Fortunately, that is likely to be sufficient for analysis of other high-resolution IR spectra we have measured at room temperature, given the signal-to-noise limitations. For example, McKellar et al [18] analysed transitions up to K_a = 13 (with $J \leq 23$) for ν_7, K_a = 10 for ν_8, and K_a = 11 for ν_{11}. The latest parameters in table 2 can also provide reliable line positions that in the context of astrophysical observations can help with accurate calculation of Doppler shifts.

The reanalysis and fitting of previously published spectral data on deuterated species, with the aid of high level DFT calculations at the B2PLYPD3/aug-cc-pVTZ level, illustrate the helpful synergy between experiment and theory. With far fewer transitions available for the deuterated species, it was not possible to fit all the centrifugal distortion terms and yet their contribution is non-negligible even in levels with small quantum numbers. Centrifugal distortion values were obtained by extrapolating from observed experimental values of the parent isotopologue, and scaling by the B2PLYPD3 computed ratio found for that particular species. This treatment improved standard

deviations for the fitted rotational transitions and the refined values of B and C rotational constants were revised by up to 0.10 MHz, corresponding to a 0.002 amu Å^2 change in I_b or I_c. That is significant in the context of subsequent structure determinations where a standard deviation of 0.0006 amu Å^2 could be attained.

The structural analyses of propynal illustrate the formidable challenge that equilibrium structure determination can present. A structure fit using the $R_m^{(1)}$ model was moderately successful. The fitted c_b and c_c coefficients help to reduce the residual standard deviation to 0.0032 amu Å^2, improved by a factor of 20 compared to the R_0 structure fit, and account for most of the zero-point motion effects. However, residuals were observed to vary systematically with the position of ^{13}C-substitution, a trend consistent with ½ $\Sigma\alpha$ values from both B2PLYPD3 and DSDPBEP86 calculations. The C2 and C3 atoms of propynal happen to be located the same distance from the b-principal axis, so that the B (and C) rotational constants of ^{13}C2 and ^{13}C3 species are almost identical. Consequently, corrections from the c_b and c_c terms cannot treat appropriately the differences stemming from ^{13}C2 or ^{13}C3 substitution, and neither can the d_α terms of an $R_m^{(2)}$ fit.

Omitting either ^{13}C2 or ^{13}C3 species and then averaging the results provides one solution to the problem, but it seems preferable to apply small geometric corrections so that all species may be incorporated in one fit that predicts all the rotational constants. Here, apparently insignificant r_{C2C3} distance corrections of +0.000085 Å to ^{13}C2 and -0.000085 Å ^{13}C3 species accomplished that. The standard deviation of 0.00062 amu.Å^2 and a range of other indicators including consistency with theoretical R_e geometries results suggest that the fit is reliable. This empirical approach is similar in essence to that employed in the $R_m^{(1L)}$ and $R_m^{(2L)}$ models, where the Laurie correction is employed in recognition of bond distance changes involving hydrogen, typically, r_0(CH) – r_0(CD) ≈ 0.003 Å. D/H substitution has a significant effect because of the large fractional change in reduced mass, μ, for relevant vibrations. Assuming the rest of the molecule is heavy in comparison, the fractional change in ($\mu^{-1/2}$) associated with a notional ^{13}C/^{12}C substitution may be approximated as *ca*. 26 times smaller than for D/H. In line with this, the applied r_{C2C3} corrections are an order of magnitude smaller than the Laurie D/H correction, suggesting they are within physically realistic bounds. Unlike D/H atoms that are always terminal with a single bond, the variety of bonding arrangements for carbon makes it unlikely that any generalised rule of thumb will apply to CX bond distance changes with ^{13}C substitution.

Watson *et al* concluded that although the c_α and d_α parameters could not account completely for zero-point motion, the $R_m^{(2)}$ model usually came much closer to equilibrium structures than the R_s substitution method [36]. Comparing the new R_s structure with "$R_m^{(2)}$ (ΔC_2C_3)" in table 5, the bond distances are quite similar with the exception of $r_{C3=O}$, and $r_{C2\text{-}C3}$. The new R_s carbonyl bond distance of 1.2127 Å is 0.0040 Å longer than in the $R_m^{(2)}$ structure, which is the expected trend for a terminal bond where one localised stretch mode is the major contributor to bond distance change from zero-point motion. On the other hand, for the mid-molecule C2C3 single bond the R_s distance is shorter by 0.0030 Å. The new R_s angles are within 0.7° of the $R_m^{(2)}$ values, the agreement much better than with Costain and Morton's R_s structure where the 180.0° constraint of angle $\theta_{HCC\ acet}$ also affected θ_{CCC}.

Overall, the $R_m^{(2)}$ structure generated may be close to an equilibrium structure, but it cannot be considered as definitive. The semi-empirical approach using computed rovibrational zero-point contributions has the potential to converge on the true structure, but this has not yet been achieved. Anharmonic frequency calculations using the two double hybrid DFT methods B2PLYPD3 and DSDPBEP86 performed well and were consistent with each other in regard to geometry, vibrational frequencies, and centrifugal distortion constants, but the predicted $\frac{1}{2}\,\Sigma\alpha_{a,b,c}$ sums needed for R_e structure determination were more divergent. In particular, the individual α_a contributions were hypersensitive to the level of theory, probably stemming from large a-axis Coriolis resonances in this near prolate molecule and their dependence on precise vibrational energy gaps. Table 3 presents rovibrational parameters for the parent isotopologue, comparing experimental with the best theoretical values (B2PLYPD3 & DSDPBEP86, along with the most recent CCSD(T)/cc-pcVTZ-F12 [35]). The $\frac{1}{2}\,\Sigma\alpha_{b,c}$ sums are a much closer match than those for the a-axis. These theoretical predictions of $\frac{1}{2}\,\Sigma\alpha_a$, ranging from -380 to -480 MHz, imply that zero-point motion changes the average angles in the molecule in such a way as to make it more nearly prolate, while the experimental $\frac{1}{2}\,\Sigma\alpha_a \approx 21$ MHz suggests there is little change in that regard. It may be surmised that the $\frac{1}{2}\,\Sigma\alpha_a$ sums represent the largest source of error in the semi-empirical structure fits attempted. Progress towards an improved semi-empirical structure may be possible with the aid of high level CCSD(T) calculations and further high-resolution band analyses can provide experimental data on rovibrational alpha constants.

Finally, considering molecular geometry as reflected in rotational constants, there is remarkably close agreement within 1 MHz between CCSD(T) and $R_m^{(2)}$ values for B_e and C_e while A_e are out by a few hundred MHz (though this is still within 0.5%). These observations suggest that the bond distances are very well predicted by theory but the bond angles are not yet optimal, a conclusion that accords with the structural comparison of table 5.

Supplemental Data

Supplemental data includes tables with: a summary of linewidths and default experimental uncertainties used in different spectral regions; an index of the SPFIT files made available with explanatory note; experimental vs computed anharmonic vibrational band positions and optimised geometries at the B2PLYPD3/aug-cc-pVTZ and DSDPBEP86/aug-cc-pVTZ levels; comparison of experimental and extrapolated quartic centrifugal distortion parameters for ^{13}C and ^{18}O substituted isotopologues; molecular constants for aldehyde deuterated propynal species from refits; and residuals (obs. – calc.) from the "$R_m^{(2)}$ (ΔC_2C_3)" structure of table 4. In addition, the predicted spectrum of the parent isotopologue is available in standard .cat format [27] from the Lille Spectroscopic Database (https://lsd.univ-lille.fr).

Acknowledgements

We are grateful to Dominique Appadoo and the staff at the Australian synchrotron THz/Far-IR beamline for facilitating the FTIR measurements. We acknowledge a La Trobe University Scholarship for MR. Quantum chemical calculations have been carried out using Australia's

National Computing Infrastructure (NCI), project k02. LM, RM and JCG thank the Programme National “Physique et Chimie du Milieu Interstellaire” (PCMI) of CNRS/INSU with INC/INP co-funded by CEA and CNES.

References

[1] W.M. Irvine, R.D. Brown, D.M. Cragg, P. Friberg, P.D. Godfrey, N. Kaifu, H.E. Matthews, M. Ohishi, H. Suzuki, H. Takeo, A New Interstellar Polyatomic Molecule: Detection of Propynal in the Cold Cloud TMC-1, Astrophys. J. 335 (1988) L89. https://doi.org/10.1086/185346.

[2] M. Ohishi, N. Kaifu, Chemical and physical evolution of dark clouds Molecular spectral line survey toward TMC-1, Faraday Discuss. 109 (1998) 205–216. https://doi.org/10.1039/A801058G.

[3] J.M. Hollis, P.R. Jewell, F.J. Lovas, A. Remijan, H. Møllendal, Green Bank Telescope Detection of New Interstellar Aldehydes: Propenal and Propanal, Astrophys. J. 610 (2004) L21. https://doi.org/10.1086/423200.

[4] J.M. Hollis, A.J. Remijan, P.R. Jewell, F.J. Lovas, Cyclopropenone (c-H_2C_3O): A New Interstellar Ring Molecule, Astrophys. J. 642 (2006) 933. https://doi.org/10.1086/501121.

[5] M.A. Requena-Torres, J. Martín-Pintado, S. Martín, M.R. Morris, The Galactic Center: The Largest Oxygen-bearing Organic Molecule Repository, Astrophys. J. 672 (2008) 352. https://doi.org/10.1086/523627.

[6] R.A. Loomis, B.A. McGuire, C. Shingledecker, C.H. Johnson, S. Blair, A. Robertson, A.J. Remijan, Investigating the Minimum Energy Principle in Searches for New Molecular Species—the Case of H2C3O Isomers, Astrophys. J. 799 (2015) 34. https://doi.org/10.1088/0004-637X/799/1/34.

[7] J.-C. Loison, M. Agúndez, N. Marcelino, V. Wakelam, K.M. Hickson, J. Cernicharo, M. Gerin, E. Roueff, M. Guélin, The interstellar chemistry of H_2C_3O isomers, Mon. Not. R. Astron. Soc. 456 (2016) 4101–4110. https://doi.org/10.1093/mnras/stv2866.

[8] C.N. Shingledecker, S. Álvarez-Barcia, V.H. Korn, J. Kästner, The Case of H_2C_3O Isomers, Revisited: Solving the Mystery of the Missing Propadienone, Astrophys. J. 878 (2019) 80. https://doi.org/10.3847/1538-4357/ab1d4a.

[9] J.A. Howe, J.H. Goldstein, Microwave Spectrum of Propiolic Aldehyde, J. Chem. Phys. 23 (1955) 1223–1225. https://doi.org/10.1063/1.1742245.

[10] C.C. Costain, J.R. Morton, Microwave Spectrum and Structure of Propynal (H–C≡C–CHO), J. Chem. Phys. 31 (1959) 389–393. https://doi.org/10.1063/1.1730364.

[11] R.C. Benson, R.S. Scott, W.H. Flygare, Molecular g values, magnetic susceptibility anisotropies, and molecular quadrupole moments in propynal, J. Phys. Chem. 73 (1969) 4359–4363. https://doi.org/10.1021/j100846a057.

[12] G. Winnewisser, The ground state of propynal, J. Mol. Spectrosc. 46 (1973) 16–24. https://doi.org/10.1016/0022-2852(73)90023-4.

[13] A.I. Jaman, R. Bhattacharya, D. Mandal, A.K. Das, Millimeterwave Spectral Studies of Propynal (HCCCHO) Produced by DC Glow Discharge and *Ab Initio* DFT Calculation, J. At. Mol. Phys. 2011 (2011) e439019. https://doi.org/10.1155/2011/439019.

[14] J. Barros, D. Appadoo, D. McNaughton, E.G. Robertson, C. Medcraft, R. Plathe, P. Roy, L. Manceron, The rotational spectrum of propynal in the 250–700GHz range using coherent synchrotron radiation Fourier transform spectrometry, J. Mol. Spectrosc. 307 (2015) 44–48. https://doi.org/10.1016/j.jms.2014.12.011.

[15] R.D. Brown, P.D. Godfry, Stark effect measurements of molecular dipole moments, Aust. J. Chem. 37 (1984) 1951–1954. https://doi.org/10.1071/ch9841951.

[16] H. Jones, Infrared-microwave double-resonance and two-photon experiments on propynal with CO2 lasers, J. Mol. Spectrosc. 81 (1980) 21–36. https://doi.org/10.1016/0022-2852(80)90327-6.

[17] M. Takami, K. Shimoda, Infrared-microwave double resonance of propynal by using the 3.51 μm He-Xe laser, J. Mol. Spectrosc. 59 (1976) 35–42. https://doi.org/10.1016/0022-2852(76)90039-4.

[18] A.R.W. McKellar, J.K.G. Watson, L.-K. Chu, Y.-P. Lee, The ν7, ν8, and ν11 bands of propynal, C_2HCHO, in the 650cm^{-1} region, J. Mol. Spectrosc. 252 (2008) 230–238. https://doi.org/10.1016/j.jms.2008.09.002.
[19] M. Takami, Millimeter-wave spectrum of DCCCHO in the ground vibrational state, J. Mol. Spectrosc. 80 (1980) 301–306. https://doi.org/10.1016/0022-2852(80)90142-3.
[20] W.D. Langer, A.A. Penzias, 12C/ 13C Isotope Ratio across the Galaxy from Observations of 13C 18O in Molecular Clouds, Astrophys. J. 357 (1990) 477. https://doi.org/10.1086/168935.
[21] A. Jabri, L. Kolesniková, E.R. Alonso, I. León, S. Mata, J.L. Alonso, A laboratory rotational study of the interstellar propynal, J. Mol. Spectrosc. 372 (2020) 111333. https://doi.org/10.1016/j.jms.2020.111333.
[22] H. McNab, G. Morel, E. Stevenson, A Short, Convenient Synthesis of Propynal†, J. Chem. Res. Synop. (1997) 207–207. https://doi.org/10.1039/A700453B.
[23] J.C. Sauer, Propiolaldehyde, Org. Synth. 36 (1956) 66. https://doi.org/10.15227/orgsyn.036.0066.
[24] O. Zakharenko, R.A. Motiyenko, L. Margulès, T.R. Huet, Terahertz spectroscopy of deuterated formaldehyde using a frequency multiplication chain, J. Mol. Spectrosc. 317 (2015) 41–46. https://doi.org/10.1016/j.jms.2015.09.005.
[25] L. Margulès, B.A. McGuire, C.J. Evans, R.A. Motiyenko, A. Remijan, J.C. Guillemin, A. Wong, D. McNaughton, Submillimeter-wave spectroscopy and the radio-astronomical investigation of propynethial (HC≡CCHS), Astron. Astrophys. 642 (2020) A206. https://doi.org/10.1051/0004-6361/202038230.
[26] L.S. Rothman, I.E. Gordon, Y. Babikov, A. Barbe, D. Chris Benner, P.F. Bernath, M. Birk, L. Bizzocchi, V. Boudon, L.R. Brown, A. Campargue, K. Chance, E.A. Cohen, L.H. Coudert, V.M. Devi, B.J. Drouin, A. Fayt, J.-M. Flaud, R.R. Gamache, J.J. Harrison, J.-M. Hartmann, C. Hill, J.T. Hodges, D. Jacquemart, A. Jolly, J. Lamouroux, R.J. Le Roy, G. Li, D.A. Long, O.M. Lyulin, C.J. Mackie, S.T. Massie, S. Mikhailenko, H.S.P. Müller, O.V. Naumenko, A.V. Nikitin, J. Orphal, V. Perevalov, A. Perrin, E.R. Polovtseva, C. Richard, M.A.H. Smith, E. Starikova, K. Sung, S. Tashkun, J. Tennyson, G.C. Toon, Vl.G. Tyuterev, G. Wagner, The HITRAN2012 molecular spectroscopic database, J. Quant. Spectrosc. Radiat. Transf. 130 (2013) 4–50. https://doi.org/10.1016/j.jqsrt.2013.07.002.
[27] H.M. Pickett, The fitting and prediction of vibration-rotation spectra with spin interactions, J. Mol. Spectrosc. 148 (1991) 371–377. https://doi.org/10.1016/0022-2852(91)90393-O.
[28] J. K. G. Watson, Aspects of quartic and sextic centrifugal effects on rotational energy levels, in: Vib. Spectra Struct. Vol 6, J. R. During (Ed), Elsevier, Amsterdam, 1977: pp. 263–264. https://doi.org/10.1016/0022-2860(78)87040-9 (accessed March 13, 2023).
[29] S. Urban, K.M.T. Yamada, A Breakdown of the Watson-Type Hamiltonian for Some Asymmetric Top Molecules, J. Mol. Spectrosc. 160 (1993) 279–288. https://doi.org/10.1006/jmsp.1993.1175.
[30] D. McNaughton, E.G. Robertson, L.D. Hatherley, Resonance between the Ground Vibrational State and the Lowest Frequency Bending Mode of Thioketene, J. Mol. Spectrosc. 175 (1996) 377–385. https://doi.org/10.1006/jmsp.1996.0043.
[31] M.K. Bane, E.G. Robertson, C.D. Thompson, C. Medcraft, D.R.T. Appadoo, D. McNaughton, High-resolution Fourier-transform infrared spectroscopy of the Coriolis coupled ground state and ν7 mode of ketenimine, J. Chem. Phys. 134 (2011) 234306. https://doi.org/10.1063/1.3597775.
[32] L. Bizzocchi, V. Lattanzi, J. Laas, S. Spezzano, B.M. Giuliano, D. Prudenzano, C. Endres, O. Sipilä, P. Caselli, Accurate sub-millimetre rest frequencies for HOCO+ and DOCO+ ions, Astron. Astrophys. 602 (2017) A34. https://doi.org/10.1051/0004-6361/201730638.
[33] M.J. Frisch, G.W. Trucks, H.B. Schlegel, G.E. Scuseria, M.A. Robb, J.R. Cheeseman, G. Scalmani, V. Barone, G.A. Petersson, H. Nakatsuji, X. Li, M. Caricato, A.V. Marenich, J. Bloino, B.G. Janesko, R. Gomperts, B. Mennucci, H.P. Hratchian, J.V. Ortiz, A.F. Izmaylov, J.L. Sonnenberg, Williams, F. Ding, F. Lipparini, F. Egidi, J. Goings, B. Peng, A. Petrone, T.

Henderson, D. Ranasinghe, V.G. Zakrzewski, J. Gao, N. Rega, G. Zheng, W. Liang, M. Hada, M. Ehara, K. Toyota, R. Fukuda, J. Hasegawa, M. Ishida, T. Nakajima, Y. Honda, O. Kitao, H. Nakai, T. Vreven, K. Throssell, J.A. Montgomery Jr., J.E. Peralta, F. Ogliaro, M.J. Bearpark, J.J. Heyd, E.N. Brothers, K.N. Kudin, V.N. Staroverov, T.A. Keith, R. Kobayashi, J. Normand, K. Raghavachari, A.P. Rendell, J.C. Burant, S.S. Iyengar, J. Tomasi, M. Cossi, J.M. Millam, M. Klene, C. Adamo, R. Cammi, J.W. Ochterski, R.L. Martin, K. Morokuma, O. Farkas, J.B. Foresman, D.J. Fox, Gaussian 16 Rev. C.01, (2016).

[34] X. Song, M. Wang, C. Yang, Y. Liu, S. Ma, X. Ma, W. Pang, The molecular structure and spectroscopic properties of C_3H_2O and its isomers: An ab initio study, Spectrochim. Acta. A. Mol. Biomol. Spectrosc. 265 (2022) 120388. https://doi.org/10.1016/j.saa.2021.120388.

[35] M. Tschöpe, G. Rauhut, A theoretical study of propynal under interstellar conditions and beyond, covering low-frequency infrared spectra, spectroscopic constants, and hot bands, Mon. Not. R. Astron. Soc. 520 (2023) 3345–3354. https://doi.org/10.1093/mnras/stad251.

[36] J.K.G. Watson, A. Roytburg, W. Ulrich, Least-Squares Mass-Dependence Molecular Structures, J. Mol. Spectrosc. 196 (1999) 102–119. https://doi.org/10.1006/jmsp.1999.7843.

[37] Z. Kisiel, Least-squares mass-dependence molecular structures for selected weakly bound intermolecular clusters, J. Mol. Spectrosc. 218 (2003) 58–67. https://doi.org/10.1016/S0022-2852(02)00036-X.

[38] Z. Kisiel, PROSPE - Programs for ROtational SPEctroscopy, (n.d.). http://www.ifpan.edu.pl/~kisiel/prospe.htm (accessed March 13, 2023).

[39] A. Kraśnicki, Z. Kisiel, B.J. Drouin, J.C. Pearson, Terahertz spectroscopy of isotopic acrylonitrile, J. Mol. Struct. 1006 (2011) 20–27. https://doi.org/10.1016/j.molstruc.2011.05.050.

[40] V.W. Laurie, Note on the Determination of Molecular Structure from Spectroscopic Data, J. Chem. Phys. 28 (1958) 704–706. https://doi.org/10.1063/1.1744218.

Figures & Tables

Figure 1.

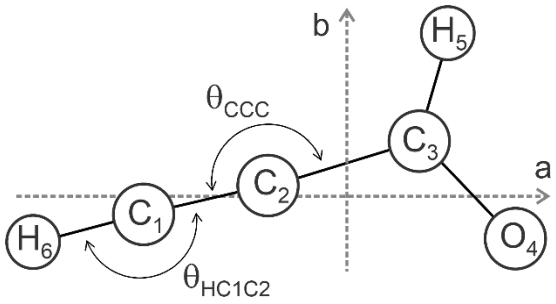

Figure 1. Structure of propynal. The near linear angles shown are slightly less than 180°.

Figure 2.

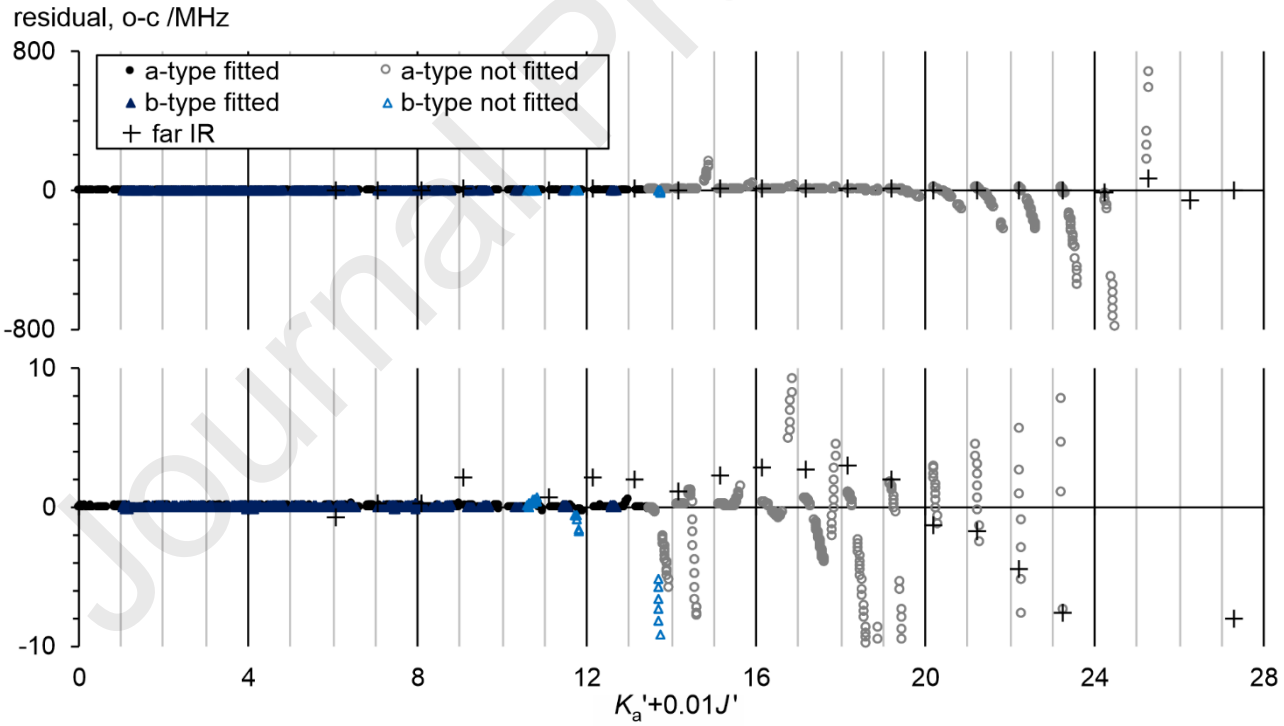

Figure 2. Residuals (observed – calculated, in MHz) from the fit of the parent isotopologue HCCCHO, plotted to show the dependence on excited state rotational quantum numbers K_a' and J'. Upper and lower traces differ only in the vertical scale.

Figure 3.

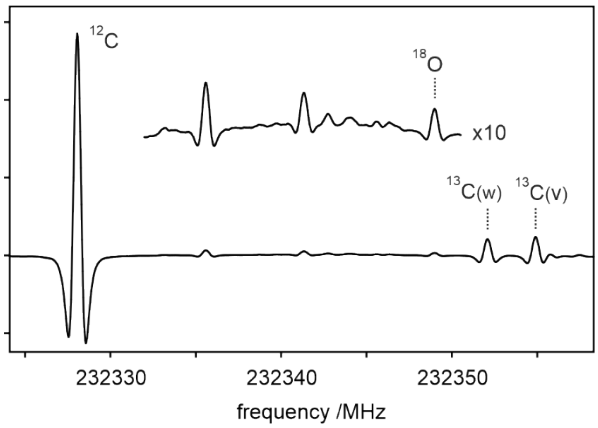

Figure 3. Section of the MMW spectrum of propynal. Some assigned transitions, all in the ground vibrational state, are labelled: ^{12}C = parent isotopologue, $22_{2,21} \leftarrow 22_{1,22}$; ^{18}O = HCCCH^{18}O, $26_{3,23} \leftarrow 25_{3,22}$; ^{13}C(w) = HCC^{13}CHO, $25_{8,17} \leftarrow 24_{8,16}$ & $25_{8,18} \leftarrow 24_{8,17}$; ^{13}C(v) = HC^{13}CCHO , $25_{7,18} \leftarrow 24_{7,17}$ & $25_{7,19} \leftarrow 24_{7,18}$.

Table 1.

Table 1. Summary of transitions included in the fit for the unsubstituted parent isotopologue.

	a-type			b-type			
Combined fit	no lines	J range	K_a range	no lines	J range	K_a range	GHz
Costain & Morton [a]	7	1-3	0-2	3	3-9	0-1	18-29
Winnewisser [a]	33	10-16	0-9	11	3-20	0-2	98-150
Jaman et al [a]	47	3-10	0-10	-			36-95
this work MMW fitted [b]	1328	16-99	0-13	1657	2-100	0-12	150-910
this work far IR	-			25	5-31	5-31	700-3500
Total fitted	1415			1696			
Other							
this work not fitted [b]	927	15-97	13-25	66	61-82	9-13	150-910
Jabri et al [21]	908	0-51	0-19	486	3-77	0-7	6-18,82-480

[a] From refs [10,12,13]. A handful of lines from these papers were omitted due to large (obs. – calc.) residuals. Also, Winnewisser transitions over 150 GHz were excluded as they were available from the current work.

[b] a-type lines were included only to J<50 for K_a = 13. b-type lines were included to K_a = 12, not 13 since the $^rP_{12}$ series does not have transitions with J < 50 within the measured range. It was also necessary to exclude b-type lines involving K_a = 10 with J > 60 due to the resonance with K_a = 2 (ν_9).

Table 2.

Table 2. Fitted molecular parameters in the s-reduced Hamiltonian [28] for the parent isotopologue of propynal, and for its ^{13}C and ^{18}O substituted isotopologues.

	^{12}C parent	H^{13}CCCHO	HC^{13}CCHO	HCC^{13}CHO	HCCCH^{18}O
A /MHz	68035.25904(49) [a]	67824.58541(177)	67960.90680(219)	66254.36409(177)	65944.792(374)
B /MHz	4826.223611(40)	4667.413259(54)	4802.709532(59)	4805.365469(46)	4612.635969(389)
C /MHz	4499.591734(40)	4360.325626(49)	4478.830826(55)	4473.430146(43)	4304.595671(389)
D_J /MHz	$1.871637(17)\times10^{-03}$	$1.749817(21)\times10^{-03}$	$1.850135(24)\times10^{-03}$	$1.821690(19)\times10^{-03}$	$1.786368(194)\times10^{-03}$
D_{JK} /MHz	-0.14772496(65)	-0.14348157(101)	-0.14841382(165)	-0.13757409(140)	-0.14921607(358)
D_K /MHz	8.990558(16)	9.030039(77)	9.135111(84)	8.404819(90)	8.7715(764)
d_1 /MHz	$-3.460680(32)\times10^{-04}$	$-3.162114(170)\times10^{-04}$	$-3.419762(173)\times10^{-04}$	$-3.426134(117)\times10^{-04}$	$-3.283327(499)\times10^{-04}$
d_2 /MHz	$-2.10110(11)\times10^{-05}$	$-1.90351(51)\times10^{-05}$	$-2.04891(25)\times10^{-05}$	$-2.16765(16)\times10^{-05}$	$-1.83596(935)\times10^{-05}$
H_J /MHz	$5.9684(29)\times10^{-09}$	$5.4606(34)\times10^{-09}$	$5.8133(38)\times10^{-09}$	$5.6639(31)\times10^{-09}$	$5.8440(315)\times10^{-09}$
H_{JK} /MHz	$-7.6954(27)\times10^{-07}$	$-7.2131(34)\times10^{-07}$	$-7.7626(40)\times10^{-07}$	$-7.1331(32)\times10^{-07}$	$-7.2238(70)\times10^{-07}$
H_{KJ} /MHz	$-6.5603(94)\times10^{-06}$	$-6.4868(61)\times10^{-06}$	$-5.3749(223)\times10^{-06}$	$-6.6015(153)\times10^{-06}$	$-8.0890(179)\times10^{-06}$
H_K /MHz	$2.41053(17)\times10^{-03}$	$2.44125(95)\times10^{-03}$	$2.40005(102)\times10^{-03}$	$2.21843(127)\times10^{-03}$	^{12}C [b]
h_1 /MHz	$2.24051(74)\times10^{-09}$	$2.01009(340)\times10^{-09}$	$2.19875(346)\times10^{-09}$	$2.18115(244)\times10^{-09}$	^{12}C
h_2 /MHz	$2.9039(39)\times10^{-10}$	$2.5809(162)\times10^{-10}$	^{12}C	^{12}C	^{12}C
h_3 /MHz	$8.3998(99)\times10^{-11}$	$7.4513(648)\times10^{-11}$	^{12}C	^{12}C	^{12}C
L_J /MHz	$-3.157(16)\times10^{-14}$	^{12}C	^{12}C	^{12}C	^{12}C
L_{JJK} /MHz	$6.341(46)\times10^{-12}$	^{12}C	^{12}C	^{12}C	^{12}C
L_{JK} /MHz	$-4.146(20)\times10^{-10}$	$-3.7417(240)\times10^{-10}$	$-4.9072(322)\times10^{-10}$	$-3.5237(227)\times10^{-10}$	^{12}C
L_{KKJ} /MHz	$-4.493(52)\times10^{-09}$	^{12}C	$-5.6010(745)\times10^{-09}$	$-2.6086(431)\times10^{-09}$	^{12}C
L_K /MHz	$-5.1634(76)\times10^{-07}$	^{12}C	^{12}C	^{12}C	^{12}C
l_1 /MHz	$-1.4119(51)\times10^{-14}$	^{12}C	^{12}C	^{12}C	^{12}C
l_2 /MHz	$-2.564(35)\times10^{-15}$	^{12}C	^{12}C	^{12}C	^{12}C
l_3 /MHz	$-1.588(16)\times10^{-15}$	^{12}C	^{12}C	^{12}C	^{12}C

l_4 /MHz	$-2.876(31)\times10^{-16}$	^{12}C	^{12}C	^{12}C	^{12}C
P_{JK} /MHz	$-6.47(27)\times10^{-17}$	^{12}C	^{12}C	^{12}C	^{12}C
P_{KJ} /MHz	$4.71(14)\times10^{-15}$	^{12}C	^{12}C	^{12}C	^{12}C
P_{KKJ} /MHz	$-1.3697(86)\times10^{-12}$	^{12}C	^{12}C	^{12}C	^{12}C
P_K /MHz	$2.68(12)\times10^{-11}$	^{12}C	^{12}C	^{12}C	^{12}C
T_K /MHz	$1.801(56)\times10^{-14}$	^{12}C	^{12}C	^{12}C	^{12}C
Δ, I_c-I_a-I_b /amu Å^2	0.17324	0.17452	0.17305	0.17589	0.17682
N (fitted)	3111	1153	1099	1089	371
Lit lines [c]	101	8	8	8	7
N (a/b-type)	1328/1682	799/346	764/327	813/268	364/0
N (omitted)	993	32	44	26	0
J-max (a/b-type)	99/100	68/61	66/60	67/67	57/-
K_a max (a/b-type)	13/12{31}[d]	16/7	15/7	17/7	15/-
MW rms /MHz	0.040	0.038	0.042	0.0355	0.0492
rms fit	0.524	0.367	0.381	0.331	0.382

[a] Values in parentheses following the fitted constants are standard errors determined using the PIFORM utility [38], in units of the least significant figure cited.

[b] ^{12}C in the table means that the centrifugal distortion constant for that isotopologue was fixed to the value of the unsubstituted parent species

[c] literature MW transitions from Costain & Morton [10], and others for the ^{12}C species, see table 1.

[d] far IR transitions extend to $K_a = 31$.

Table 3. Comparison of fitted molecular constants for the parent HCCCHO isotopologue with those from anharmonic vibrational calculations at the B2PLYPD3/aug-cc-pVTZ, DSDPBEP86/aug-cc-pVTZ and CCSD(T)/cc-pcVTZ-F12 levels.

	Experiment	**B2PLYPD3**	**DSDPBEP86**	**CCSD(T)/cc-pcVTZ-F12 (ae)** [b]
A_e /MHz	68056 [a]	67919	67710	67768
B_e /MHz	4835.6 [a]	4832.0	4814.9	4836.0
C_e /MHz	4514.8 [a]	4511.1	4495.3	4513.9
A_0 /MHz	68035	68375	68096	68247
B_0 /MHz	4826.2	4819.9	4804.3	4824.0
C_0 /MHz	4499.6	4495.6	4480.8	4498.6
½ $\Sigma\alpha_a$ /MHz	21 [a]	-456	-387	-479
½ $\Sigma\alpha_b$ /MHz	9.4 [a]	12.1	10.6	12.1
½ $\Sigma\alpha_c$ /MHz	15.3 [a]	15.5	14.4	15.3
Δ_0 /amu Å^2	0.1732	0.1731	0.1738	0.1724
D_J /MHz	1.87×10^{-03}	1.83×10^{-03}	1.82×10^{-03}	
D_{JK} /MHz	-1.48×10^{-01}	-1.49×10^{-01}	-1.49×10^{-01}	
D_K /MHz	8.99	8.77	8.82	
d_1 /MHz	-3.46×10^{-04}	-3.36×10^{-04}	-3.35×10^{-04}	
d_2 /MHz	-2.10×10^{-05}	-1.59×10^{-05}	-1.60×10^{-05}	
H_J /MHz	5.97×10^{-09}	5.73×10^{-09}	5.92×10^{-09}	
H_{JK} /MHz	-7.70×10^{-07}	-7.39×10^{-07}	-7.79×10^{-07}	
H_{KJ} /MHz	-6.56×10^{-06}	-1.10×10^{-07}	-8.60×10^{-06}	
H_K /MHz	2.41×10^{-03}	2.47×10^{-03}	2.43×10^{-03}	
h_1 /MHz	2.24×10^{-09}	2.11×10^{-09}	2.17×10^{-09}	
h_2 /MHz	2.90×10^{-10}	2.13×10^{-10}	2.19×10^{-10}	
h_3 /MHz	8.40×10^{-11}	5.84×10^{-11}	6.01×10^{-11}	

[a] From "$R_m^{(2)}$ (ΔC_2C_3)" structure of table 5.

[b] All electron calculation of Tschöpe & Rauhut [35].

Table 4.

Table 4. Molecular constants for deuterated propynal species from refitting transitions of Costain & Morton [10]. Quartic centrifugal constants without parentheses are extrapolated using anharmonic B2PLYPD3/aug-cc-pVTZ values (see text) and constrained in the fits.

	DCCCHO [a]	HCCCDO	DCCCDO	D^{13}CCCHO	DC^{13}CCHO	DCC^{13}CHO
A /MHz	66778.0847(92) [b]	51768.345(42)	51079.005(30)	66635.61 [c]	66686.03 [c]	65073.18 [c]
B /MHz	4463.79400(51)	4791.5487(47)	4429.1901(28)	4334.741(18)	4446.582(16)	4442.718(18)
C /MHz	4177.86185(49)	4378.8121(95)	4069.6650(68)	4064.069(18)	4162.410(15)	4152.525(18)
D_J /MHz	1.56800(42)×10^{-3}	1.646×10^{-3}	1.373×10^{-3}	1.475×10^{-3}	1.551×10^{-3}	1.520×10^{-3}
D_{JK} /MHz	-0.138776(10)	-0.06040	-0.06035	-0.1330(33) [d]	-0.1385(29) [d]	-0.1346(44) [d]
D_K /MHz	9.4341(14)	3.295	3.471	9.422	9.593	8.792
d_1 /MHz	-2.8921(34)×10^{-4}	-3.424×10^{-4}	-2.785×10^{-4}	-2.626×10^{-4}	-2.829×10^{-4}	-2.811×10^{-4}
d_2 /MHz	-1.7744(19)×10^{-5}	-3.661×10^{-5}	-2.769×10^{-5}	-1.455×10^{-5}	-1.587×10^{-5}	-1.673×10^{-5}
Δ, I_c-I_a-I_b /amu Å^2	0.18054	0.17932	0.18600			
N (a/b-type)	91 / 62	3 / 4	2 / 4	8 / 0	8 / 0	7 / 0
J max	37	6	7	3	3	3
K_a max	15	1	1	2	2	2
MW rms /MHz	0.050	0.030	0.018	0.064	0.056	0.062
rms fit	0.496	0.298	0.181	0.642	0.558	0.621

[a.] DCCCHO transitions from Costain & Morton [10] and Takami [19], 5 transitions with K_a >15 excluded from fit. In addition to the fitted quartic constants, four sextic constants of DCCCHO were determined (in MHz): H_{JK} = -6.564(100)×10^{-7}, H_{KJ} = -7.662(37)×10^{-6}, H_K = 2.630(60)×10^{-3}, h_1 = 5.16(21)×10^{-9}. The remaining higher order centrifugal distortion parameters were constrained to the corresponding value for the unsubstituted parent species in table 2.

[b] Values in parentheses following the fitted constants are standard errors determined using the PIFORM utility [38].

[c] The A rotational constants of D^{13}CCCHO, DC^{13}CCHO and DCC^{13}CHO are constrained to extrapolated estimates, see text.

[d] The extrapolated B2PLYPD3/aug-cc-pVTZ values for D_{JK} in MHz are -0.1387 (D^{13}CCCHO), -0.1424 (DC^{13}CCHO), and -0.1324 (DCC^{13}CHO).

Table 5.

Table 5. Comparison of structural parameters from experimental structure determinations and theoretical calculations.

	Experimental				Theory		
Parameter	**R_s Costain [a]**	**R_s new**	**b) Semi-emp**	**g) $R_m^{(2)}$ (ΔC_2C_3) [b]**	**B2PLYPD3 /aVTZ**	**DSDPBEP86 /aVTZ**	**CCSD(T) /cc-pcVTZ-F12(ae) [c]**
r C1≡C2 / Å	1.2089(8) [d]	1.2058(45)	1.2110(13)	1.2066(15)	1.2071	1.2100	1.2062
r C2-C3 / Å	1.4446(5)	1.4456(51)	1.4450(14)	1.4486(14)	1.4452	1.4495	1.4505
r C3=O / Å	1.2150(10)	1.2127(40)	1.2092(13)	1.2087(10)	1.2121	1.2120	1.2077
r C-H aldehyde / Å	1.1064(9)	1.1077(34)	1.0941(16)	1.1069(8)	1.1002	1.1018	1.0986
r C-H acet / Å	1.0553(5)	1.0568(25)	1.0554(6)	1.0578(13)	1.0615	1.0642	1.0626
θ CCC / °	178.40(17)	177.39(147)	178.56(44)	176.71(22)	177.68	177.59	177.57
θ OCC / °	123.78(17)	123.73(70)	123.76(24)	123.23(7)	123.70	123.57	123.33
θ HCC aldehyde / °	113.90(17)	114.13(67)	114.28(23)	114.43(31)	114.84	114.89	115.08
θ HCC acet / °	180.0 fixed	178.88(124)	180.21(38)	178.45(16)	178.89	178.84	178.80
c_a / amu$^{1/2}$.Å^2				0.0029(053)			
c_b / amu$^{1/2}$.Å^2				0.0336(158)			
c_c / amu$^{1/2}$.Å^2				0.0471(165)			
d_a / Å^2				-0.0029(110)			
d_b / Å^2				-0.0747(815)			
d_c / Å^2				-0.0637(834)			
fit std dev [e] /amu.Å^2			0.00273	0.00062			

[a] reference [10].

[b] A r_{C2C3} distance correction was applied to both ^{13}C2 (+0.000085 Å) and ^{13}C3 species (-0.000085 Å), refer to text for details.

[c] All electron calculation of Tschöpe & Rauhut [35].

[d] Parentheses following the geometric parameters indicate experimental uncertainties. The larger uncertainties for the new R_s structure result from inclusion of "Costain rule" errors.

[e] Fit standard deviation of the residuals in STRFIT is given by $\{ \Sigma (I_{obs} - I_{calc})^2 / (n - K) \}^{1/2}$, where n = number of I_{obs} values and K = the number of fitted parameters.

Author Statement

Evan G. Robertson: Conceptualization, Investigation, Formal analysis, Writing - Original Draft, Writing - Review & Editing.
Mahmut Ruzi: Formal analysis, Writing - Review & Editing.
Don McNaughton: Conceptualization, Writing - Review & Editing.
Laurent Margulès: Investigation, Data Curation, Writing - Review & Editing.
Roman A. Motiyenko: Investigation.
Jean-Claude Guillemin: Resources, Writing - Review & Editing.

Highlights

- Astrochemical molecule propynal (HCCCHO) is studied by millimeter wave spectroscopy
- Rarely seen, the ground vibrational state has extensive resonance perturbations
- Improved rotational constants are obtained for parent, ^{13}C and ^{18}O isotopologues
- Experimental $R_m^{(2)}$ and R_s structures are derived, consistent with high level theory

Isotopologues in natural abundance

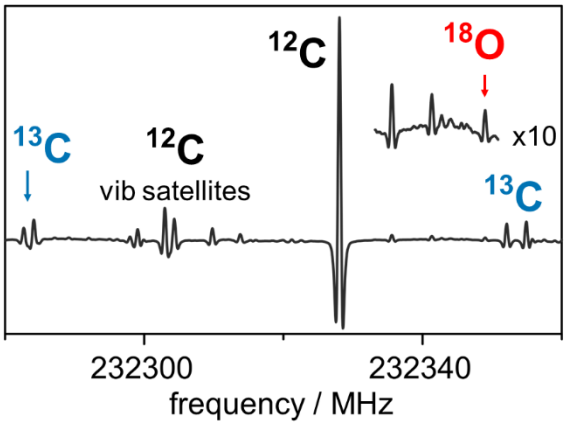

Experimental $R_m^{(2)}$ structure of propynal

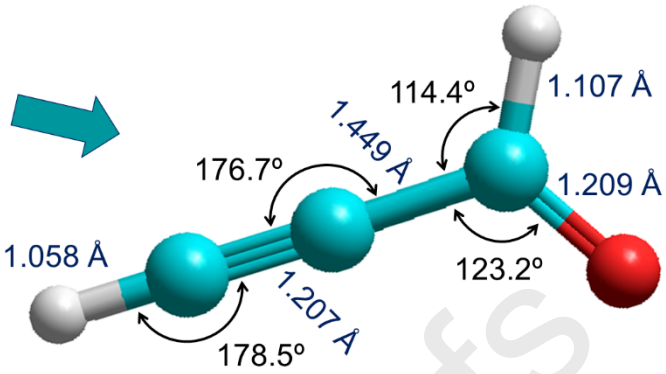

Declaration of interests

☒ The authors declare that they have no known competing financial interests or personal relationships that could have appeared to influence the work reported in this paper.

☐The authors declare the following financial interests/personal relationships which may be considered as potential competing interests: